Storm and Entrainment Effects on Tributary Sediment Loads

By Deborah H. Lee,[1] Keith W. Bedford,[2] and Chieh-Cheng J. Yen,[3] Members, ASCE

Abstract: A two-dimensional, multiclass-size sediment transport model with source/sink terms for erosion and deposition, and a sediment bed model were developed and applied to Sandusky Bay, Ohio to study the transport of fine sand, silt, and clay through the bay for June 1 to June 30, 1981. During this period, a flood carried high sediment loads from the Sandusky River to the bay. The model's simulation showed that 79.3% of the flood's sediment loads were deposited in the upper bay. Areas of net deposition and erosion compare favorably to other published results. This study showed that the dominant sediment size transported to Lake Erie is clay, and the sediment load to Lake Erie is significantly different from that measured at the U.S. Geological Survey gage at Fremont, Ohio, located upstream of the bay. Weaknesses in state-of-the-art sediment transport modeling and field measurements are discussed.

INTRODUCTION

The recent interest of water-quality analysts in determining the effects of toxic substances has renewed emphasis on predicting tributary sediment delivery rates to receiving waters. This is especially the case with tributaries that drain watersheds with both agricultural and industrial uses and where silt and clay are the dominant sediment classes. In such situations, these classes are the primary transport agent responsible for delivering toxic substances, herbicides, and pesticides to receiving waters. Many of the tributaries entering the Great Lakes are of this type. To manage the effects of pollutants, the U.S.-Canadian Boundary Water Treaty Act of 1978 requires reporting of annual pollution loads delivered to the lakes as derived from monthly averaged loading data. For the U.S. portion of the Great Lakes basin, the United States Geological Survey (USGS) maintains a system of water quality gages on these tributaries, and the regularly sampled flow and pollutant concentration data are collated into monthly loading data. USGS gages located on tributaries to Lake Erie are placed well upstream of the lake as it experiences large storm surges that cause extensive flow disruptions in the lower portions of its tributaries. Bedford and Mark (1988) used a coupled hydrodynamic and water quality model to show how the load of chloride in the Sandusky River measured at the USGS site in Fremont, Ohio from 1 June 1981–16 July 1981 compared in timing and magnitude to the chloride load delivered to Lake Erie 29 km downstream. The effect of storms was demonstrated and phase errors were pronounced, but as might be expected with a conservative substance, the phase error was the only significant loading error for that period.

It is hypothesized, however, that for sediment transport, especially for loads containing a broad range of sand, silt, and clay, significant differences

[1]Res. Hydro., Great Lakes Envir. Res. Lab., Ann Arbor, MI 48105.
[2]Prof., Dept. of Civ. Engrg., Ohio State Univ., Columbus, OH 43210.
[3]Res. Assoc., Dept. of Civ. Engrg., Ohio State Univ., Columbus, OH.

Note. Discussion open until June 1, 1994. To extend the closing date one month, a written request must be filed with the ASCE Manager of Journals. The manuscript for this paper was submitted for review and possible publication on July 29, 1992. This paper is part of the ***Journal of Hydraulic Engineering***, Vol. 120, No. 1, January, 1994. ©ASCE, ISSN 0733-9429/94/0001-0081/$1.00 + $.15 per page. Paper No. 4505.

will exist between loads and grain size distributions measured upstream versus at the receiving water. The objective of this paper is to report on a hydrodynamic and sediment transport model study of the same region and for the same time period just mentioned that investigates this hypothesis.

HYDRODYNAMIC AND SEDIMENT TRANSPORT MODELS

Hydrodynamic Model

The hydrodynamic model (Bedford and Mark 1988) consists of a simple two-dimensional, nonlinear model for predicting free surface position and distributions of vertically averaged horizontal velocity. The model is based on the depth-averaged continuity equation

$$\frac{\delta \eta}{\delta t} + \frac{\delta}{\delta x}(\eta + h)U + \frac{\delta}{\delta y}(\eta + h)V = 0 \quad \ldots\ldots\ldots\ldots\ldots\ldots\ldots (1)$$

and depth-averaged momentum equations written for the x- and y-directions, respectively

$$\frac{\delta U}{\delta t} + U\frac{\delta U}{\delta x} + V\frac{\delta U}{\delta y} - fV + \frac{\tau_b^x}{\rho_w H} = -g\frac{\delta \eta}{\delta x} + \frac{\tau_s^x}{\rho H} \quad \ldots\ldots\ldots\ldots (2)$$

$$\frac{\delta V}{\delta t} + U\frac{\delta V}{\delta x} + V\frac{\delta V}{\delta y} - fU + \frac{\tau_b^y}{\rho_w H} = -g\frac{\delta \eta}{\delta y} + \frac{\tau_s^y}{\rho H} \quad \ldots\ldots\ldots\ldots (3)$$

U and V are the depth-averaged velocities in the x- and y-directions; η = the free surface fluctuation and h = the water depth such that the sum of η and h = H, the total water depth; f = the frictional shear stress; ρ_w = the density of water; τ_b = the bottom shear stress due to currents; g = the gravitational acceleration; and τ_s the surface wind shear stress. The equations are discretized by finite differences, defined on a rectangular grid, and solved at discrete points in the flow field according to the alternating direction implicit method (Leendertse 1967). This model was used successfully in forecasting Lake Erie storm surges (Dingman and Bedford 1986) and, within the limits of available data, the hydrodynamics of Sandusky Bay (Bedford and Mark 1988).

Multiclass Sediment Transport Model

For each of three grain size classes, i, the depth-averaged convective-dispersive sediment transport equation

$$\frac{\delta HC_i}{\delta t} + \frac{\delta}{\delta x}(HUC_i) + \frac{\delta}{\delta y}(HVC_i) = \frac{\delta}{\delta x}\left(HK_x\frac{\delta C_i}{\delta x}\right)$$

$$+ \frac{\delta}{\delta y}\left(HK_y\frac{\delta C_i}{\delta y}\right) + S_{ei} - S_{di} \quad \ldots\ldots\ldots\ldots\ldots\ldots\ldots\ldots\ldots (4)$$

is solved. C_i = the concentration of the ith grain size class; K_x and K_y = dispersion coefficients, and S_{ei} and S_{di} = source/sink terms for entrainment and deposition, respectively. The assumption that transported material does not influence the water motion allows the hydrodynamic equations to be uncoupled from the sediment transport equation. The calculated hydrodynamic values are used as knowns in solving the sediment transport equation at each time step.

The entrainment model for S_{ei} distinguishes between unconsolidated and consolidated bottom material. For cohesive unconsolidated bottom material for each class, the formula of Parchure and Mehta (1985) is used:

$$S_{ei} = \varepsilon_{0i} \exp \alpha_i \left(\frac{\bar{\tau}_b}{\tau_{cei}} - 1 \right) \quad \ldots\ldots (5)$$

where α_i and ε_{0i} = coefficients for each size class and reflect erodability. $\bar{\tau}_b$ = the bed shear due to currents and waves, while τ_{cei} is the critical erosion shear stress for class size i.

For consolidated and all noncohesive sediments, (6) due to Ariathurai and Arulanandan (1978) is used:

$$S_{ei} = E \left(\frac{\bar{\tau}_b}{\tau_{cei}} - 1 \right) \quad \ldots\ldots (6)$$

where E = an erodability coefficient with dimensions of $M/L^2/T$. This term is set to zero when $\bar{\tau}_b < \tau_{cei}$. These forms were selected because of their credible use in previous models and the availability of empirical knowledge about the various coefficients. The deposition term, S_{di}, developed by Krone et al. (1977) for flow deposition is:

$$S_{di} = \frac{P_i V_{si} C_i}{h} \quad \ldots\ldots (7)$$

where V_{si} = the settling velocity of the class size given by Krone et al. (1977) as

$$V_{si} = K_{si} C_i^{4/3} \quad \ldots\ldots (8)$$

In (8), K_{si} = an empirical coefficient dependent upon sediment type. The probability of particles remaining deposited, P_i, is given as

$$P_i = \left(1 - \frac{\bar{\tau}_b}{\tau_{cdi}} \right) \quad \ldots\ldots (9)$$

where τ_{cdi} = the critical deposition shear stress. The deposition term is set to zero when $\bar{\tau}_b > \tau_{cdi}$.

Shear Stress Calculation

The bottom shear stress responsible for entrainment consists of components due to the mean current field and the effect of wind driven gravity waves. The total shear is given as (Sheng and Lick 1979)

$$\bar{\tau}_b = \frac{1}{T_s} \int_0^{T_s} |\bar{\tau}_c + \bar{\tau}_w| \, dt \quad \ldots\ldots (10)$$

where $\bar{\tau}_b$ = the bottom shear vector averaged over one wave cycle. $\bar{\tau}_c$ = the shear stress vector due to the current

$$\bar{\tau}_c = \frac{\rho_w g}{C_c^2} (\bar{V}^2)^{1/2} |\bar{\mathbf{V}}| \quad \ldots\ldots (11)$$

where the velocity vector, $\bar{\mathbf{V}}$, is the resultant from the x and y vertically

averaged components (U and V). The bottom shear due to the gravity waves, $\bar{\tau}_w$, is parameterized as

$$\bar{\tau}_w = \rho_w f_w U_m^2 \cos^2\left(\frac{2\pi t}{T_s}\right) \quad \ldots\ldots\ldots\ldots\ldots\ldots\ldots\ldots\ldots\ldots\ldots\ldots\ldots\ldots\ldots\ldots (12)$$

where f_w = a wave friction factor, U_m = the maximum orbital velocity at the bottom as calculated from linear wave theory, and T_s = the significant wave period. All wave parameters were estimated by the spectral based forecasting methods in the U.S. Army Corps of Engineers *Shore Protection Manual* (1984). $\bar{\tau}_w$ is resolved into x and y model components from wind direction components. The integration in (10) was reduced to four special cases: (1) $\bar{\tau}_c < \bar{\tau}_{w\max}$ and $\bar{V} > 0$; (2) $\bar{\tau}_c < \bar{\tau}_{w\max}$ and $\bar{V} < 0$; (3) $\bar{\tau}_c <<< \bar{\tau}_{w\max}$; and (4) $\bar{\tau}_{w\max} <<< \bar{\tau}_c$, where $\bar{\tau}_{w\max} = \rho_w f_w U_m^2$. The resulting integrations are given in Lee (1986). This procedure does not account for nonlinear interaction between wave and current generated shear stress (Glenn and Grant 1987; Grant and Madsen 1986). It was selected because it allowed closed form estimates of shear unlike the iterative solutions required of the nonlinear schemes.

Multiclass-size Bed Model

The erosion and deposition terms for suspended sediment are calculated simultaneously with the bed entrainment and deposition terms. Incorporating bed models is a necessary feature of sediment transport models with the models of Krone et al. (1977), Sheng (1983), Onishi and Thompson (1984), Hayter and Mehta (1982), and Ziegler and Lick (1988) being among those reported. The bed model used here is similar to Krone et al. (1977) except that it accounts for unconsolidated and consolidated sediments as does Hayter and Mehta (1982). Unlike Hayter and Mehta (1982) this model includes multigrain sizes. The bed is idealized to consist of n layers with each layer containing up to five different grain size classes, each of which is represented by the median grain size. The bed characteristics are described by the thickness of the top layer, the average particle density of each layer, and the critical erosion shear stress for each layer for each sediment class. Sediment characteristics are described by the erodability coefficient, the settling velocity, and critical deposition shear stress.

The first $n - 1$ layers of the n bed layers contain 1–m unconsolidated layers and $m + 1$ to $n - 1$ consolidated layers. The nth layer is the nonerodible layer and has infinite extent.

Erosion occurs when $\bar{\tau}_b > \tau_{cei}$ and sediment of class i exists in the top bed layer. The potential sediment mass to be removed for each class is given by

$$M_{ei} = S_{ei}(\Delta t)(A) \quad \ldots\ldots\ldots\ldots\ldots\ldots\ldots\ldots\ldots\ldots\ldots\ldots\ldots\ldots\ldots\ldots (13)$$

for the finite difference cell area (A), during a time interval Δt, the model time step. If the available mass is less than M_{ei}, then all of the mass is entrained. If the available mass is greater than M_{ei}, then the mass equivalent to M_{ei} is entrained, and the difference remains in the top layer. The next bed layer can erode if: (1) All sediment (from all classes) has been removed from the top layer; (2) the critical erosion shear stress of a class in that layer is exceeded; and (3) sediment of that class is available.

Similarly, deposition amounts can also be calculated:

$$M_{di} = S_{di}(t_d)(A) \qquad (14)$$

The parameter, t_d, is the deposition integration time that represents the time period between updating deposition events in the model. It may be as small as Δt.

After the erosion or deposition event, the new layer properties are calculated: thickness, total mass, sediment mass of each class size, and the average particle density. Thickness increases, T_n, from deposition are calculated as

$$T_n = \frac{(\rho_s - \rho_w)}{\rho_s(\rho_b - \rho_w)} \frac{\text{mass}_d}{A} \qquad (15)$$

where ρ_s = the particle density, and ρ_b = the sediment bulk density. The

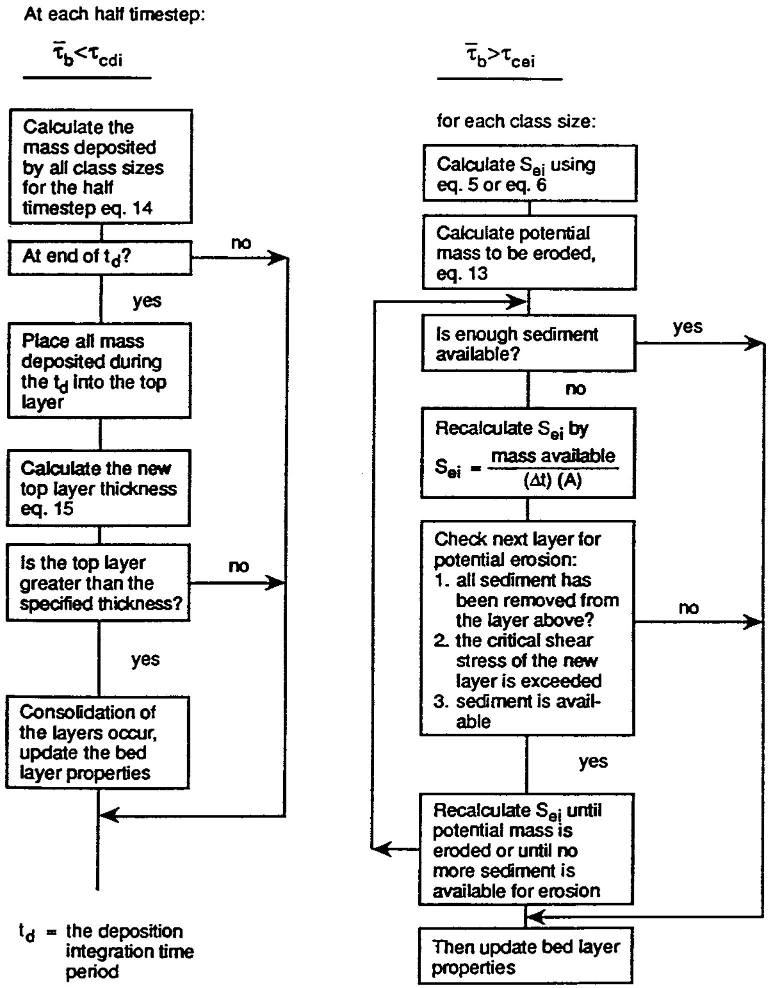

FIG. 1. Sediment Bed Model Flow Chart

average particle density of each layer is calculated as the average of the particle densities weighted by the mass of each class size deposited to the total mass deposited, $mass_d$. For each layer, the thickness, the total mass, the mass of each class size, and the weighted average particle density are recorded. When the top layer is filled, consolidation of the layers to the next higher order of aggregation occurs, i.e., the top layer moves to the second, etc., until the $n - 1$ layer is added to the nth layer. Fig. 1 is a flowchart of the bed model implementation.

ADAPTATION TO SANDUSKY BAY/RIVER SYSTEM

Setting

Fig. 2 depicts the region to be simulated, along with the transects A, B, and C, in Sandusky Bay. These three transects distinguish the river from the upper bay, the upper and lower bay, and the lower bay and the lake respectively. The bay is shallow, being on the average 3 m in the lower bay and 1.6 m in the upper bay. The bay is 25.4-km long and has a total surface area of 147 km^2 (83.5 km^2 in the upper bay, 63.5 km^2 in the lower bay). The average water level ranged, for the simulation period, between 0.90 and 1.10 m above datum, which is 173.35 m.

Lake Erie affects the bay in many ways including seiche mode coupling. Lake Erie has seiche modes of 14.4-, 9.1-, 5.9-, and 4.2-hour longitudinal modes and a 3.0-hour transverse mode (Dingman and Bedford 1984), which are imposed upon the bay. Additionally, the bay has 3.0- and 1.7-hour modes (Bedford 1989). Due to storm surges and mode oscillations, flow reversals can occur at the confluence. The main inflow to the bay is the Sandusky River with an average flow rate of 2.24 (10^6) m^3/day from the 3,681-km^2 watershed (Lloyd 1974). The hydrographs are double peaked, separated by as much as 48 hours.

Simulation Conditions and Data

Sandusky Bay was parameterized by a computational grid of 1,260 square cells each with a length of 375 m. The nodal definitions are in the staggered grid configuration (Leendertse and Gritton 1971). The maximum number of cells in the longitudinal bay axis (Fig. 2) is 60 while the maximum number of cells in the cross stream direction is 20.

Hydrometeorological data required by the hydrodynamic model was obtained for June 1 to July 17, 1981. This period was selected as water quality data were collected at 34 locations (Fig. 2) by Richards and Baker (1982) in the Sandusky River, bay, and nearshore area during two flood events. Suspended solids data measured during June 12 to June 25 were used to verify the results of the sediment transport model simulations. Wind speed, direction, air and water temperature data were obtained from the National Weather Service in Cleveland, Ohio. The wind shear data, calculated by the stability dependent method of Schwab (1980), is portrayed in Fig. 3(*a*) and demonstrates several forceful wind events. The hourly water levels measured at the National Ocean Service gage at Marblehead are shown in Fig. 3(*a*) and a small 0.5-m surge is evident, a once-a-year event (Bedford and Mark 1988). Using flow data from the Fremont USGS gage and the HEC-1 computer program, the flows at transect A, the upstream simulation boundary condition, were synthesized and are displayed in Fig. 3(*b*). Two double peak events are noted: the first a 20-year return period event and the second a three-year return period event.

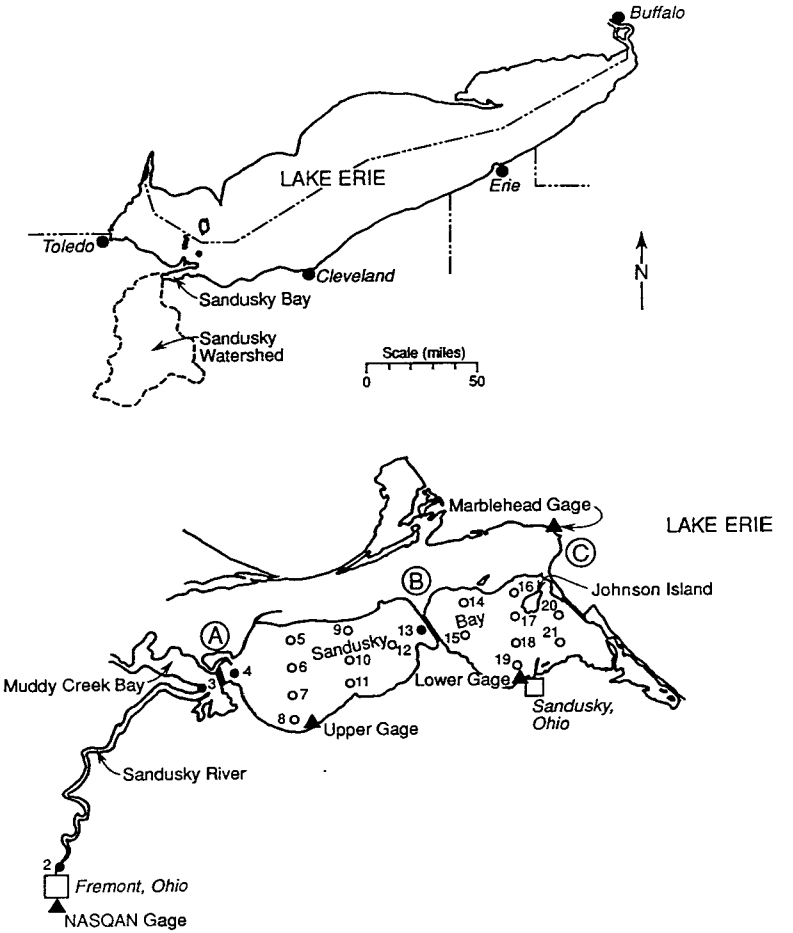

FIG. 2. Lake Erie/Sandusky Bay Setting and Bay Sampling Sites and Transect Configuration

Data required by the sediment transport and bed models were estimated from a variety of sources. Total suspended solids at transect A were measured over the simulation period at the Fremont gage and they closely traced the flow hydrograph. A survey done by the Ohio Department of Natural Resources ("Water" 1966) related grain size distribution at the Fremont gage to sediment discharge. Using the HEC-1 simulation and a grain size dependent settling velocity as per (7), (8), and (9), the sediment classes were routed downstream to transect A. Only deposition was allowed to occur during this brief riverine reach; the contribution of resuspended riverbed sediments was thought to be small in comparison to the total suspended load. The resulting time traces for three grain size classes are plotted in Fig. 4 with the measured concentrations at station 4 shown as a check on this boundary condition.

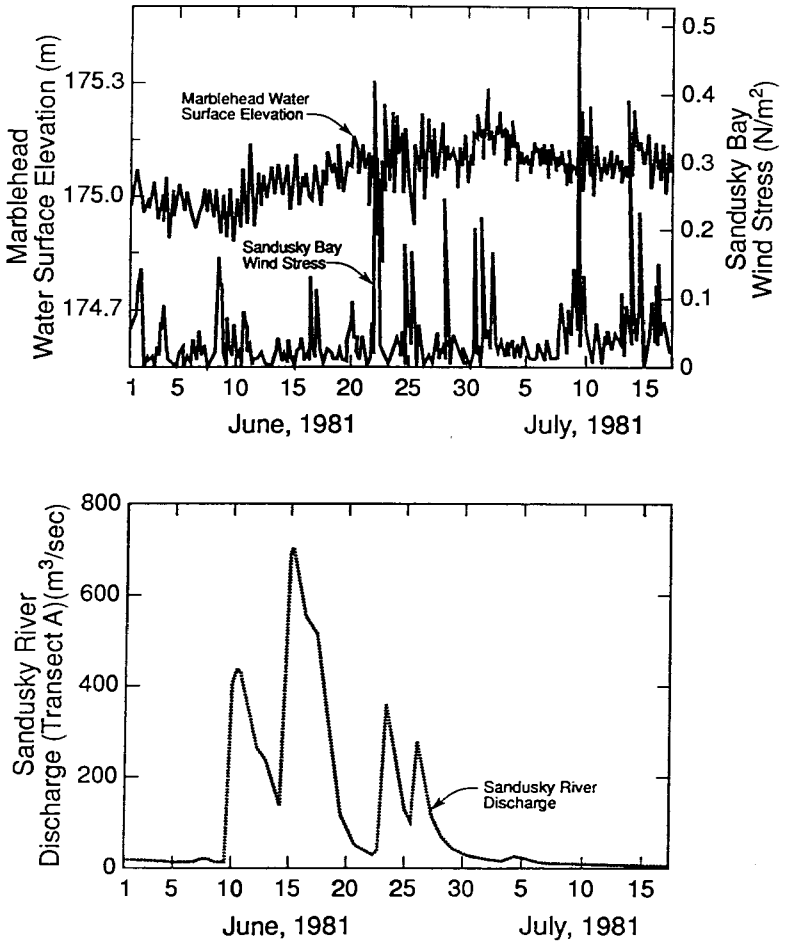

FIG. 3(*a*). Wind Shear and Marblehead Water Level Time Series; and (*b*) Sandusky River Inflow Time Series

The initial bed sediment distribution was compiled from reports by Carter et al. (1975), Herdendorf (1978), Richards and Baker (1982), the Ohio Department of Transportation ("Boring" 1962), and the Ohio Department of Natural Resources ("Water" 1966). Due to the lack of sediment layer data, a two-layer model was used with properties as mapped in Fig. 5.

Transport Model Coefficient Calibration and Selection

The hydrodynamic calculations reproduced the Sandusky Bay free mode surface response observed at the upper bay water level gage (Fig. 6) by calibration of the bottom friction factor. Spectral analysis of the one-hour running average water level model predictions were compared to theoretically calculated spectra by Bedford et al. (1983) and the spectra determined from the measured data. The predicted results reproduced all five Lake Erie modes within the bay and the first two free modes of Sandusky Bay.

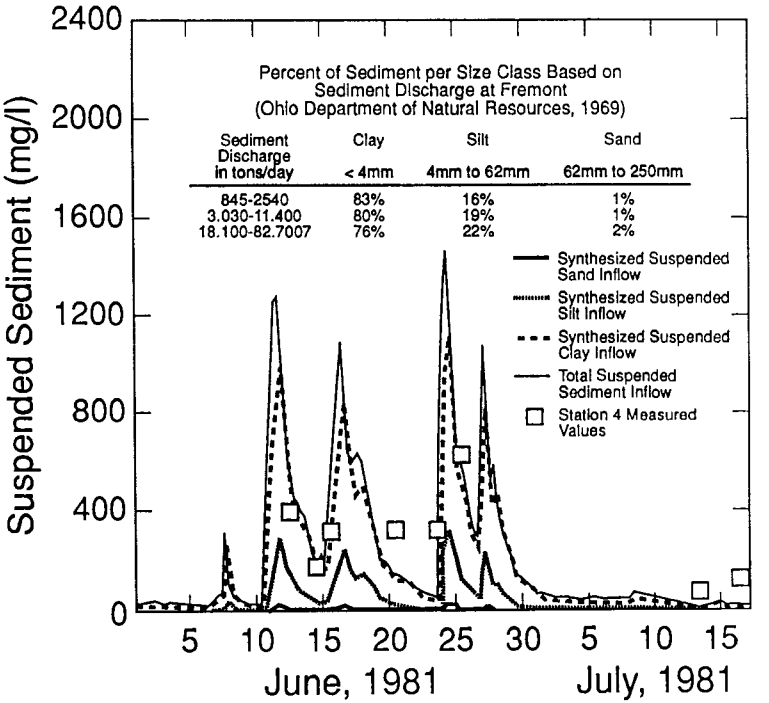

FIG. 4. Sandusky River Sediment Inflow and Grain Size Time Series

Oscillatory activity is portrayed down to a three-hour resolution. The writers realize that reproducing water levels does not ensure correct velocity fields, but no current meter data were available.

The dispersion coefficients in the transport model were determined by Bedford and Mark (1988) through the calibration of simulations, for June 1 to July 16, 1981, with data measured at stations 4–21. Adjustments in the coefficients were made until the best fit was achieved, as measured by a skill test procedure (Dingman and Bedford 1986). Optimum results were achieved with constant values of 40.0 m^2/s for the longitudinal coefficient and 0.4 m^2/s for the lateral coefficient.

Sediment Transport Model Coefficient Selection

The sediment transport coefficient values were selected primarily from the published works of the original model developers. Table 1 summarizes the various parameters, their values, and the reference for each. A similar summary table of the bed model coefficients is in Table 2. Note that although the silt and clay parameters for deposition (i.e., the settling velocities) are different, the erosion parameters have the same values for these classes. The values selected represent those derived for cohesive mass erosion, not particle erosion, and thus values representative of sediments containing both classes were selected. The initial parameter selection did not account for the effects of flocculation on settling velocity.

Three simulations of June 1 to July 13, 1981 were calculated and compared

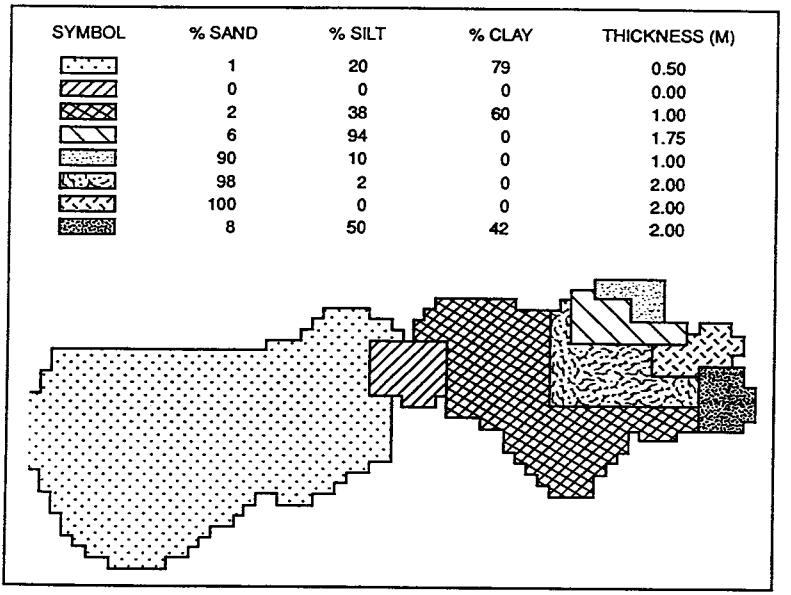

FIG. 5. Initial Distribution and Volume of Sandusky Bay Bed Sediments

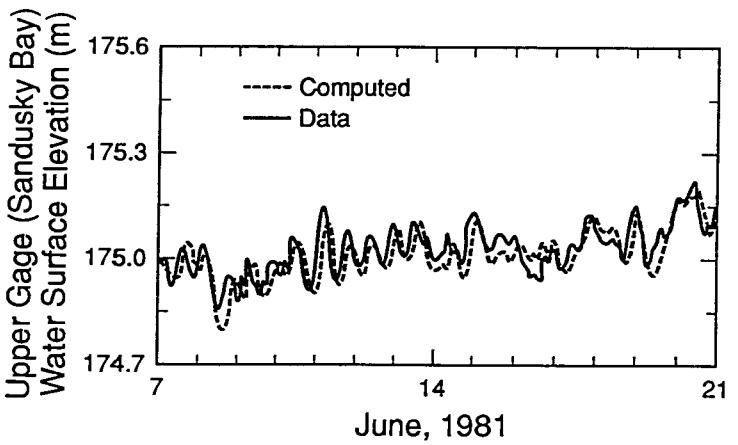

FIG. 6. Upper Sandusky Bay Water Level Time Series (Bedford and Mark 1988)

via a nonparametric skill test (Dingman and Bedford 1986) to the measured data from sites 4–21 (Fig. 2). The three simulations were distinguished as per parameters in Table 3. The nonparametric skill test assigned scores in proportion to the relative error of the simulated value to the measured value such that a high score reflected a poor simulation and vice versa. The score for a perfect prediction was zero, while ten was the point value assigned the worst prediction. The worst possible average aggregate score was 1,800, while the best was zero. Skill test scores for each simulation were performed for each station and for each date that data were collected. These scores

TABLE 1. Initial Erosion, Deposition, and Bed-Layer Input Parameters and Sources

Parameter (1)	Fine sand (2)	Silt (3)	Clay (4)	Source of data (5)
Class size, in mm	0.125–0.062	0.062–0.004	≤0.004	Herdendorf (1978), Water (1966), and Carter et al. (1975)
Settling velocity, V_s (m/s)	2.8×10^{-2} (Stoke's law)	1.0×10^{-5} (Fukuda and Lick 1980)	1.2×10^{-6} (Fukuda and Lick 1980)	Stoke's law and Fukuda and Lick (1980)
Erodability coefficient, E (kg/m²/s)	1.0×10^{-5} (Vanoni 1975)	2.72×10^{-5} (Sheng and Lick 1979)	2.72×10^{-5} (Sheng and Lick 1979)	Vanoni (1975) and Sheng and Lick (1979)
Erodability coefficient, α_i	—	15	15	Hayter and Mehta (1982)
ε_{0i} (kg/m²/s)	—	2.2×10^{-7}	2.2×10^{-7}	Hayter and Mehta (1982)
Critical shear stress, τ_{cdi} (N/m²)	0.09 (Herdendorf 1978)	0.02 (Krone et al. 1977)	0.02 (Krone et al. 1977)	Herdendorf (1978) and Krone et al. (1977)
Particle density, ρ_s (kg/m³)	2,650	2,650	2,650	Vanoni (1975)

TABLE 2. Initial Bed Model Parameters and Sources

Parameter (1)	Bulk density (kg/m^3-ρ_b) (2)	Critical Shear Stress for Erosion (N/m^2-τ_{cdi})		
		Sand (3)	Silt (4)	Clay (5)
Layer 1	1,090	0.10	0.05	0.05
Layer 2	1,114	0.10	0.15	0.15
Source of data	Krone et al. (1977)	Vononi (1975)	Krone et al. (1977)	Krone et al. (1977)

TABLE 3. Deposition Parameterization for Three Simulations

Simulation (1)	Settling velocity (2)	Critical shear stress for deposition (3)
1	Silt: 1.0×10^{-5} m/s	0.02 N/m^2
	Clay: 1.2×10^{-6} m/s	0.02 N/m^2
2	Silt: 1.0×10^{-4} m/s	0.02 N/m^2
	Clay: 1.2×10^{-5} m/s	0.02 N/m^2
3	Silt: 1.0×10^{-4} m/s	0.04 N/m^2
	Clay: 1.0×10^{-5} m/s	0.04 N/m^2

were then compiled into a simulation score for each station, a total score for each simulation, and total scores for each simulation in each basin. Table 4 contains the aggregate scores for the total station and basin simulation scores. Simulation 1 employed settling velocities indicative of unflocculated sediment. The results when compared to the measured values showed that the simulated values were much higher, with a total basin score of 585 points, with the upper and lower basin scores of 272 and 315 respectively. Simulation 2 was performed with settling velocities indicative of "flocculation effects." After the conclusion of this research, further evidence for the importance of flocculation in fresh water was presented by Tsai et al. (1987) lending support to the rationale for simulation 2. An improvement occurred in both total basin and subbasin scores.

Simulation 3 was performed using the settling characteristics of simulation 2 and a higher critical shear stress for deposition, again addressing the question of settling of clay and silt particles. Skill scores were improved with the total, upper, and lower bay scores being respectively 475, 212, and 263.

Simulation 3, with improved clay and silt deposition characteristics was the best simulation of those attempted. The evidence gathered in these three simulations suggests that incorporating improved representation for the deposition behavior of clays and silts is an important model requirement. The average station score in the lower bay was consistently higher than the upper bay scores in all three simulations. The lower bay is the primary coupling region between Lake Erie seiche and surge activity and the bay, and long wave oscillatory activity is extensive throughout the lower bay for the simulation time period. The lower bay is a very complicated mixing zone for the transport of materials, and the higher (poorer) skill scores reflect this complexity.

TABLE 4. Aggregate Skill Test Scores for Simulations

Station (1)	Station Aggregate Score/Average		
	Simulation 1 (2)	Simulation 2 (3)	Simulation 3 (4)
	(*a*) Upper Bay		
4	28/4.6	35/5.8	35/5.8
5	15/7.5	7/3.5	6/3.0
6	26/5.2	28/5.6	28/5.6
7	20/10.0	20/10.0	20/10.0
8	11/5.5	15/7.5	16/8.0
9	20/10.0	17/8.5	14/7.0
10	53/6.6	39/6.5	40/6.7
11	20/10.0	20/10.0	19/9.5
12	39/7.8	18/3.6	18/3.6
13	40/6.7	30/5.0	16/2.7
[Basin subtotal/average]	272/7.2	229/6.0	212/5.5
	(*b*) Lower Bay		
14	12/4.0	18/6.0	20/6.3
15	61/7.6	60/7.5	54/6.7
16	16/8.0	14/7.0	14/7.0
17	70/8.8	67/8.3	54/6.8
18	35/8.8	32/8.0	30/7.5
19	30/7.5	17/4.2	21/5.3
20	62/8.8	47/6.7	47/6.7
21	27/6.8	25/6.2	23/5.7
[Basin subtotal/average]	313/7.8	280/7.0	263/6.5
[Total score]	585/7.5	509/6.5	475/6.0

TABLE 5. Total Sediment Transported through Transects A, B, and C for June 1 to June 30, 1981

Transect (Fig. 2) (1)	Total (t) (2)	Sand (t) (3)	Silt (t) (4)	Clay (t) (5)
C	51,133	13,659 (26.7%)	6,047 (11.8%)	31,427 (61.5%)
B	50,494	−573 (−1.1%)	1,615 (3.2%)	49,450 (97.9%)
A	242,812	8,200 (3.4%)	57,213 (23.6%)	177,399 (73.0%)
Fremont	372,194	—	—	—

MONTHLY LOAD RESULTS

Total Load

The results of simulation 3 were used to estimate the sediment load through transect C for June 1 to June 30, 1981. The calculated sediment concentrations for each grain size class as well as the velocity were stored at each model time step (5 min) at the three transects A, B, and C (Fig. 2). The mass flux at each transect was calculated at each time step and summed over the month to form a total load passing through each transect for the period. Table 5 summarizes these estimated loads.

From these results, a number of features are apparent. First, it is estimated

that 129,382 t (1 t equals 1,000 kg), or 35% of the Fremont load, has been deposited in the river channel before it enters the upper bay. Secondly, the upper bay is a net deposition zone in that 192,320 t have been deposited. The lower bay, however, is unique in that approximately equal loads enter and leave it through transects B and C. Comparing the Fremont load to the load estimated to pass into Lake Erie reveals that for this one month time period only 13.7% reaches Lake Erie, a significant difference. More revealing than total loading rates is the estimated loading rate for each grain size class.

Grain Size Class Monthly Loads

As shown in Table 5, the load entering the upper bay is composed of clays (73.0%) with an additional fraction (23.6%) of silts. Very little of the load entering the upper bay is sand. The load passing transect B, however, is quite different in both magnitude and grain size class distribution. The entire load of sand and most of the silt load entering the upper bay has been deposited within the upper bay. There is a small net transport of sand from the lower to the upper bay during flow reversals due to seiche events, but it is not believed to be significant. The only grain size class transported to the lower bay is the clay fraction, with 127,950 t (72%) having been deposited in the upper bay. The upper bay is primarily a deposition zone for sand and silts. This is consistent with the results reported in Carter et al. (1975).

By contrast, the lower bay is quite different. As mentioned, the total loads at B and C are essentially equivalent, but the load at transect B was almost entirely clay (97.9%), while the load at transect C consists of 61.5% clays and 38.5% of sand and silt. The lower bay is a very active resuspension area; the large percentage of transported sand and silt originate from resuspension of initially specified bed material. Some of the clay transported from the upper bay is deposited, but this occurs at the outlet from transect B and around Johnson Island, not in the main channel to transect C where the resuspension of the sand and silt occur. In the analysis of the response of the bed, this behavior is further discussed.

The class size results indicate that complex mechanisms interact throughout the month of June that deliver loads to Lake Erie that are different in magnitude and grain size composition from that measured at the Fremont, Ohio, USGS gage.

Total Load Fluxes

The time traces of the fluxes for the total sediment load at transects A, B, and C are shown in Figs. 7, 8, and 9, respectively. Fig. 7 portrays the Sandusky River tributary load into the upper bay. Figs. 8 and 9 show that both the transects B and C sediment flux time series contain persistently low-amplitude oscillations until about 12 June, 1981. Such oscillatory activity persists due to the Lake Erie free seiche modes, which have insufficient time to die away between the expected storm occurrence intervals (Irish and Platzman 1962; Dingman and Bedford 1984). The amplitudes of the sediment flux traces then increase as the river flood carries sediment into the bay. The time series are further amplified by the Lake Erie storm surge on 21 June 1981. The strong oscillations introduced at the transects by the storm surge lasted from 21 June to 29 June, 1981. Storm surge effects are not noticed in the transect A flux time series.

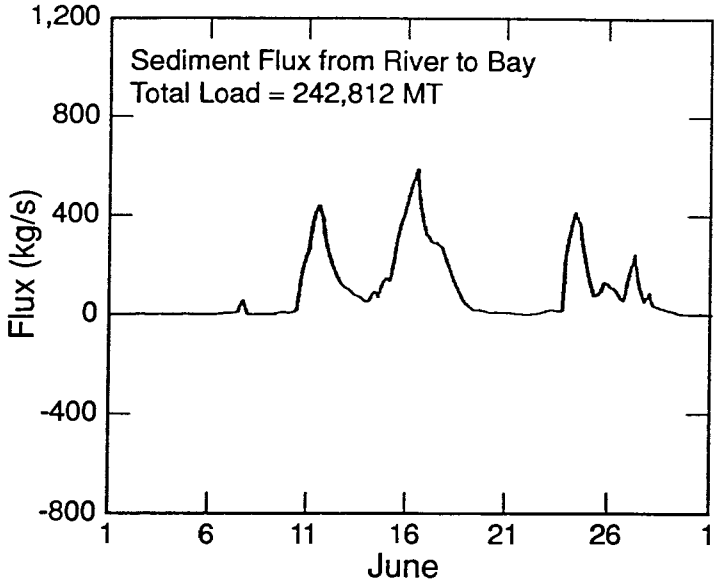

FIG. 7. Time Trace of Total Sediment Flux: Transect A

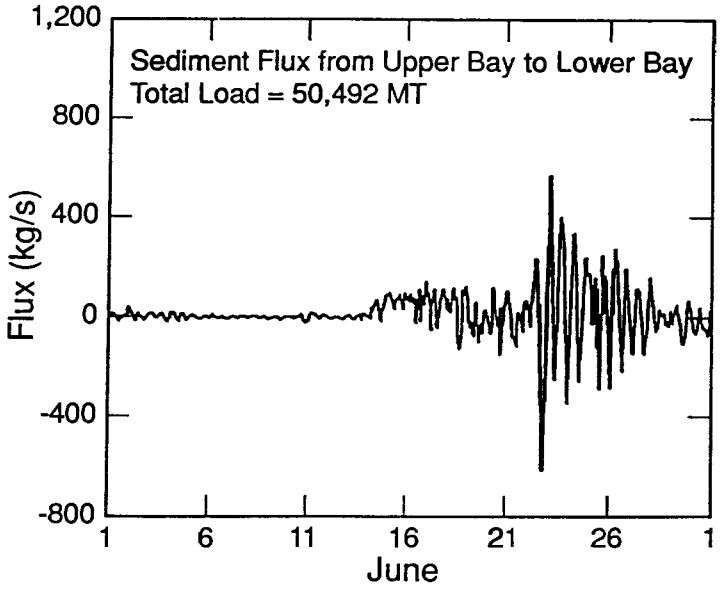

FIG. 8. Time Trace of Total Sediment Flux: Transect B

RESPONSE OF BED

With such significant amplitude and grain size redistribution occurring as the load passes through each transect, it is necessary to examine where the

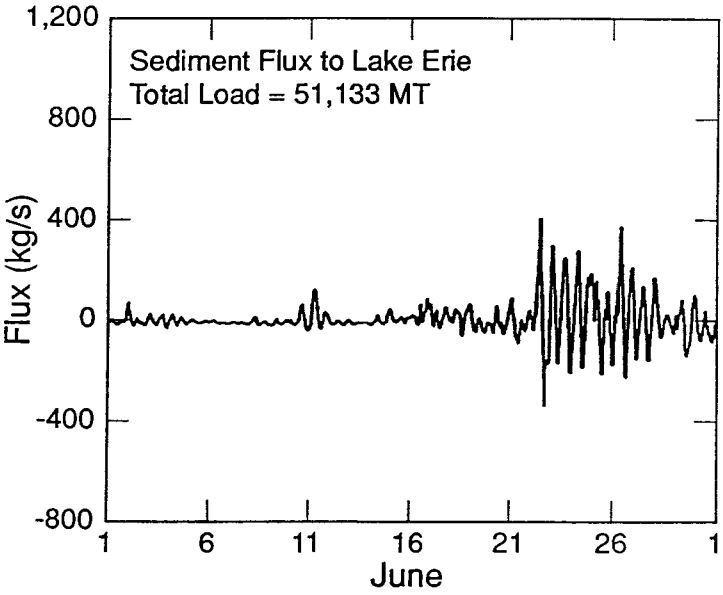

FIG. 9. Time Trace of Total Sediment Flux: Transect C

zones of deposition and entrainment within Sandusky Bay are and what is the net effect on the bottom. Fig. 10 contains a map of the net erosion and deposition zones for total sediment during the entire simulation, while Figs. 11–13 contain similar plots for the sand, silt, and clay fractions. Fig. 10 shows that significant deposition occurs downstream of transect A with weaker net deposition occurring over the entire upper bay.

The most intense erosion areas occur at transects B and C with as much as 11 cm of material removed from these regions. The degree of erosion predicted at these sites, coupled with the knowledge that the highest stresses occur in transect B, lead one to believe that the initially specified volumes of material at this site were erroneously large. Scour should keep the transect B and C channels relatively clean. Another area of erosion is located on a line from Johnson Island to the city of Sandusky.

While only speculating at this point, it is probably more than a coincidence that the Johnson Island–City of Sandusky line of erosion (Fig. 10), is close to the S2 mode line (Bedford and Mark 1988) that contains the maximum horizontal velocity excursions and stresses. From linear wave theory, it is expected that this region would be a zone of high acceleration—a direct correlate with shear. Other areas of erosion occur along the south and north shores; these areas correspond to zones where wave induced resuspension is high. The patterns of total sediment erosion and deposition from Fig. 10 compare favorably with upper bay long-term erosion and deposition patterns presented in Carter et al. (1975).

With regard to the grain size classes, sand erosion occurs along the shores and the constrictions at transects B and C and the Johnson Island line. The increasing sand erosion in the lower bay corresponds to bottom deposits there. The sand erosion pattern repeats itself for silt but there is no erosion at transect C as there are no local deposits. Clay erosion is almost nonexistent

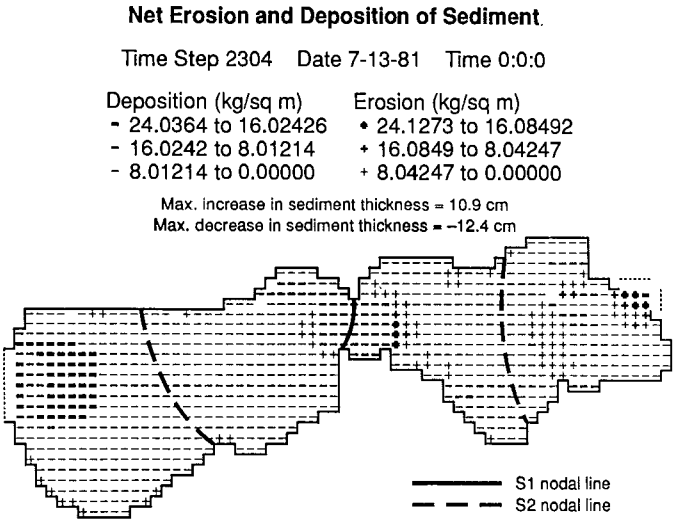

FIG. 10. Net Sandusky Bay Erosion and Deposition

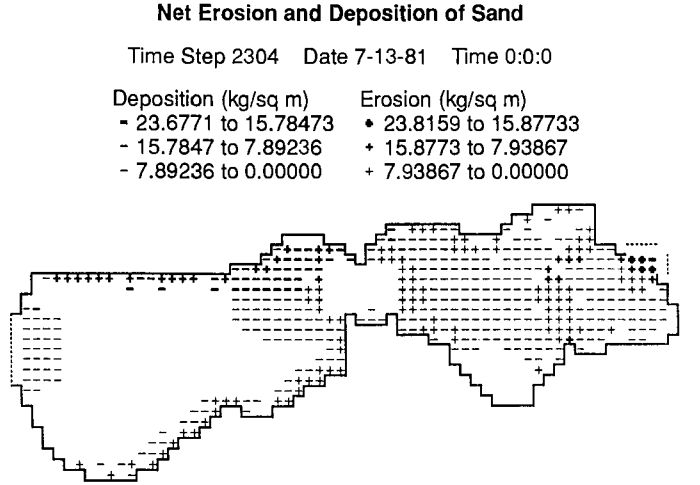

FIG. 11. Net Sandusky Bay Sand Erosion and Deposition

in the lower bay as there are no substantial bed sources. No sand is deposited in the upper bay. Some sand deposition occurs weakly in the lower bay, while strong deposition of silts and clays occurs in the upper bay with weaker deposition occurring in the lower bay.

Fig. 14 shows the net change in bed thickness resulting over the simulation period. The greatest net deposition occurs in the upper bay with the largest increases in sediment thickness (11 cm) reflecting the bulk densities specified for the bed layers. The values selected were for fluid mud. However, over

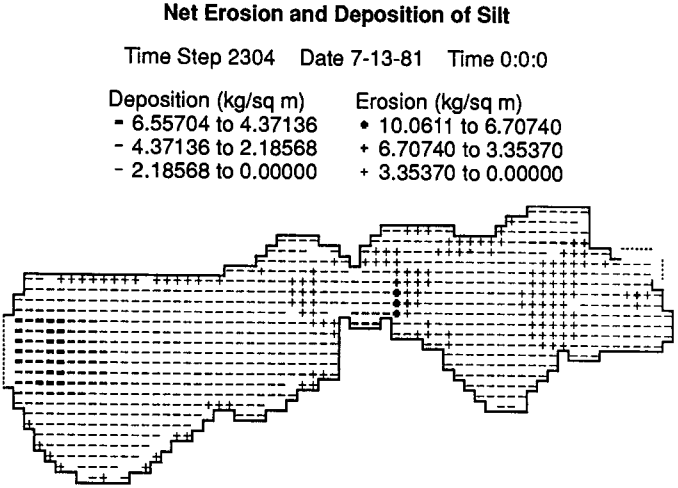

FIG. 12. Net Sandusky Bay Silt Erosion and Deposition

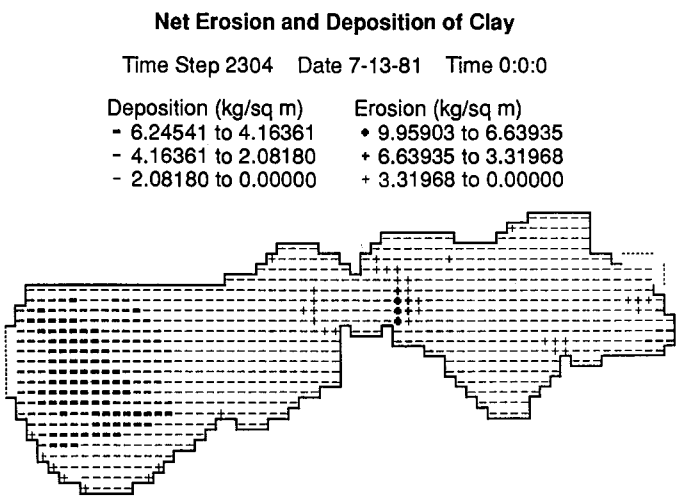

FIG. 13. Net Sandusky Bay Clay Erosion and Deposition

time these sediments should compact to a higher density and yield a somewhat thinner deposition thickness.

Carter et al. (1975) calculated an annual upper bay deposition rate of 4.3 mm/year and a measured rate of 5.5 mm/year, which was based upon a long-term average annual sediment inflow of 284,000 t and an average annual shore erosion load of 209,000 t. The deposition thickness for this simulation period can be estimated in a similar fashion. Assuming a depositional area of 56.8 km^2, a sediment density of 1.9 g/cm^3 and the predicted upper bay deposited mass of 198,805 t gives an average thickness of 1.87 mm. Given that most of the sediment mass is delivered to the bay during spring storms

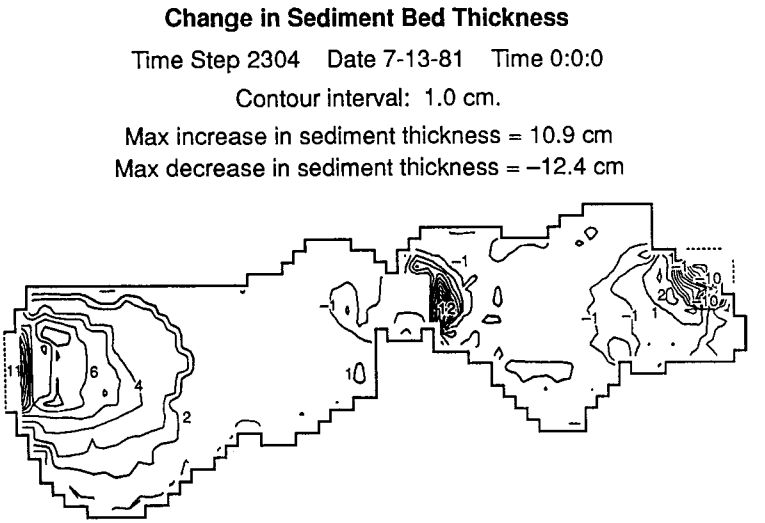

FIG. 14. Net Change in Sandusky Bay Bed Sediment Thickness

from March through June, this seems a reasonable model deposition prediction.

ANALYSIS

The model results presented here, while not from a spatially complex, three-dimensional model, nevertheless contain a variety of interacting processes parameterized by a number of empirical functions. From comparisons with field data, a number of positive model results can be identified particularly as to how the effects of short-term hydrodynamic events like seiches affect longer term, monthly tributary load estimates. The bay's modeled water level fluctuations agreed with the available data and correctly portrayed the effects of the stability dependent wind shear and the water level seicheing effects imposed by Lake Erie.

With regard to the suspended and bed sediment models, the general spatial and temporal distributions matched the measured values somewhat successfully, as indicated by the nonparametric skill test scores (Table 4). Calculations in the interior portions of the bay were most successful while those near the shore or near very dramatic changes in plan form geometry fared less well. The inclusion of the wind waves in the entrainment shear stress is an absolute requirement, especially in shallow waters such as these, and is responsible for the correctly calculated nearshore resuspension. That the nearshore entrainment was in many cases underpredicted might be due to the use of the wave-current shear stress formulae used.

The sediment entrainment and deposition patterns in the upper bay appeared to correlate with the data for June 1981, and the long-term data collected about deposition rates and bottom grain size distributions. That the calculated deposition rates were in qualitative agreement with longer term observations is heartening, particularly as this model required settling velocity adjustments for improved results. The upper bay grain size deposition behavior was also in agreement with existing data. The upper bay is

not as complex a transport situation as the lower bay since the Lake Erie and Sandusky oscillation modes are not as powerful. The upper bay calculation then was reasonable given the extreme uncertainty in the data and empirical coefficients.

The lower bay suspended and bed sediment distributions are, to say the least, complex. The interaction of the Sandusky and Lake Erie mode structures is a dominant feature. The distributions of sediment are satisfactorily calculated near the confluence with the upper bay, and the net loading rate analysis indicates the correct entrainment and sorting effect of silt and sand occurs in the lower bay. The erosion and deposition patterns in the lower bay also reflect this seiche-induced sorting behavior. It is extremely interesting to note the correlation of the lower bay S2 null oscillation line with the bed erosion pattern (Fig. 10). Indeed, the entire region east of this null oscillation line is a mixing zone for Lake Erie and Sandusky Bay waters. Being such a complex hydrodynamic and topographic domain, the lower bay simulation was at best marginal.

The lower bay complexity exposes a number of flaws in this modeling exercise as well as sediment modeling in general. First, the two-dimensional, vertically integrated model used here will not allow the full vertical profile resolution necessary for highly accurate lower bay mixing zone analysis. Secondly, improved dispersion or turbulence models will need to be employed, especially as much more highly refined (spatially) data from satellites (Lyons et al. 1988) are employed and expose much more spatial variability in the data than what is measured here. However, the two most important flaws in this model are those that exist for this class of model in general, i.e., the degree of empiricism in the subcomponent models and the corresponding lack of field data or data acquisition methods with which to obtain the required data.

There is a considerable amount of empiricism in these models; for each grain size equation, over seven empirical coefficients must be specified. The skill tests documented the importance of the settling characteristics and suggested the utility of considering flocculation effects. Many of these subcomponent models have been constructed from laboratory exercises and little field verification of them has been done. Only within the last several years have field results on entrainment (Bedford et al. 1987) of noncohesive soils been performed. The field verification of these subcomponent models should become a primary consideration.

A final flaw in these studies is the lack of certain types of instrumentation required to collect some of the field data required by these models. The use of satellite data will improve data precision and is to be encouraged. Recent work by Lyons et al. (1988) demonstrates the successful use of Landsat and Advanced Very High Resolution Radiometer (AVHRR) data for Sandusky sediment patterns. Displayed in these remotely sensed images is the same lower bay mixing zone line seen in the bottom erosion plots (Fig. 10) and the S2 null line configuration.

However, many of the data required by these models simply are never routinely measured or cannot be measured. No better example of this exists than in the bed model structure where data are required on the number of layers, their volume and particle size distribution, in situ moisture content, all pieces of information that can't be measured in situ during the course of the other field measurements without physically collecting a sample, destroying the required data. The state of measurement systems for the required bed data is poor.

CONCLUSIONS

From the model analysis performed, and to within the limits imposed by the data, the following conclusions and results are warranted: (1) There is considerable difference in the quantity and grain size distribution of the monthly average sediment load that reaches the Lake Erie nearshore zone compared to what is operationally measured at the USGS gage in Fremont, Ohio; (2) this difference calls into question the calculation of monthly nearshore sediment loading rates calculated from the USGS gages and that a more comprehensive survey over the course of one or more years should be undertaken to determine if this is a systematic or random difference; (3) the impact of storm surges, seiches, and Sandusky Bay free mode oscillations on the monthly average nearshore load is pronounced and causes grain size sorting by selective entrainment and deposition; (4) the effect of the fundamental 14-hour Lake Erie free mode is dominant and sampling of these tributary loads at a period of four hours or less is necessary to properly account for its effect (the sampling interval should not coincide with a fundamental free mode period); and (5) a considerable amount of work must be done to improve the accuracy of the empirical models and coefficients used by the models and of necessity must come a new generation of instrumentation for measuring the required data. This is particularly true for the bed model and the possible effects of flocculation or coagulation on settling velocities.

ACKNOWLEDGMENTS

This research was supported in part by NOAA–Ohio Sea Grant research project No. NA84AA-D-00079 R/EM-4. D. Lee was supported by an Ohio State University Graduate Fellowship. The support is greatly appreciated. Finally, the writers wish to thank P. Richards for his data and counsel. This is GLERL contribution No. 809.

APPENDIX I. REFERENCES

Ariathurai, R., and Arulanandan, K. (1978). "Erosion rates of cohesive soils." *J. Hydr. Engrg.*, ASCE, 104(2), 279–283.

Bedford, K. (1989). "Storms and the occurrence of a turbidity interface/maxima in a fresh water estuary." *Proc. Int. Symp. on Sediment Transp. Modeling*, H. Shen, ed., ASCE, New York, N.Y., 106–111.

Bedford, K., and Mark, D. (1988). "The effect of storms and gage location on a tributary load estimate." *J. Envir. Engrg.*, ASCE, 114(2), 352–366.

Bedford, K., Prater, M., Mattox, W., and Herdendorf, C. (1983). "The effect of Lake Erie/Sandusky Bay seiche oscillations on the formation of Sandusky Bay." *OWRT-USGS Project Completion Report*, Water Res. Ctr., Ohio State Univ., Columbus, Ohio.

Bedford, K., Wai, O., Libicki, C., and Vanevra, R. (1987). "Sediment entrainment and deposition measurements in Long Island Sound." *J. Hydr. Engrg.*, ASCE, 113(10), 1325–1342.

Boring logs for bridge number OTT-2-2904, Sandusky Bay bridge. (1962). Ohio Department of Transportation, Columbus, Ohio.

Carter, C., Benson, D., and Guy, D., Jr. (1975). "Shoreline and bathymetric changes in and around Upper Sandusky Bay since 1905." D. Baker, W. Jackson, and B. Prater, eds., *Sandusky River Basin Symposium*, International Joint Commission.

Dingman, J., and Bedford, K. (1984). "The Lake Erie response to the January 1978 Cyclone." *J. Geophysical Res.*, 89, 6427–6455.

Dingman, J., and Bedford, K. (1986). "Skill tests and parametric statistics for model evaluation." *J. Hydr. Engrg.*, ASCE, 112(2), 124–141.

Fukuda, M., and Lick, W. (1980). "The entrainment of cohesive sediments in freshwater." *J. Geophysical Res.*, 85(5), 2813–2824.
Glenn, S., and Grant, W. (1987). "A suspended sediment stratification correction for combined wave current flows." *J. Geophysical Res.*, 92(8), 8244–8264.
Grant, W., and Madsen, O. (1986). "The Continental Shelf bottom boundary layer." *Annual Review of Fluid Mech.*, 18, 265–306.
Hayter, E., and Mehta, A. (1982). "Modeling estuarial fine sediment transport for tracking pollutant movement." *Tech. Report 82/009*, Univ. of Florida Coastal Engrg. Lab., Gainesville, Fla.
Herdendorf, C. E. (1978). "Description of sediment samples and cores from the Michigan and Ohio waters of Lake Erie." *Tech. Report 85*, Ctr. for Lake Erie Area Res., Coll. of Biological Sci., Ohio State Univ., Columbus, Ohio.
Irish, S., and Platzman, G. (1962). "An investigation of the meteorological conditions associated with extreme wind tides on Lake Erie." *Monthly Weather Review*, 90, 39–47.
Krone, R., Ariathuri, R., and MacArthur, R. (1977). "Mathematical model of estuarial sediment transport." *Tech. Report D-77-12*, U.S. Army Corps of Engrs., Dredged Material Res. Program, Vicksburg, Miss.
Lee, D. (1986). "The development of a multi-class size sediment transport model and its application to Sandusky Bay, Ohio," MS thesis, Ohio State University, Columbus, Ohio.
Leendertse, J. (1967). "Aspects of a computational model for long-period wave propagation." *Rand Corporation Memorandum RM-5295-PR*, Rand Corporation, New York, N.Y.
Leendertse, J., and Gritton, E. (1971). "Water quality sanitation model for well mixed estuaries and coastal seas." *Rand Corporation Memorandum R-709-NYC*, Rand Corporation, New York, N.Y.
Lloyd, J. (1974). "The hydrologic evaluation of surface water adjacent to and including Sandusky Bay for a proposed power plant," MS thesis, Ohio State Univ., Columbus, Ohio.
Lyons, J., Bedford, K., Yen, C. C., Lee, D., and Mark, D. (1988). "Determinations of suspended sediment concentrations from multiple day Landsat and AVHRR data." *Remote Sens. Environ.*, 25(1), 107–115.
Onishi, Y., and Thompson, F. L. (1984). *Mathematical simulation of sediment and radionuclide transport in coastal waters.* Office of Nuclear Regulatory Research, U.S. Nuclear Regulatory Commission, Washington, D.C.
Parchure, T. M., and Mehta, A. J. (1985). "Erosion of soft cohesive sediment deposits." *J. Hydr. Engrg.*, ASCE, 111(18), 1308–1326.
Richards, R., and Baker, D. (1982). "Assimilation and flux of sediments and pollutants in the Sandusky River estuary, Sandusky Bay, and adjacent nearshore zone of Lake Erie." *Supplementary Report NA8ORD00038*, National Oceanic and Atmospheric Administration Office of Marine Pollution Assessment, Rockville, Md.
Schwab, D. (1980). "Simulation and forecasting of Lake Erie storm surges." *Monthly Weather Review*, 106, 453–460.
Sheng, P. (1983). "Mathematical modeling of three dimensional coastal currents and sediment dispersion." *Technical Report CERC-83-2*, U.S. Army Corps of Engineers, Vicksburg, Miss.
Sheng, P., and Lick, W. (1979). "The transport and resuspension of sediments in a shallow lake." *J. Geophysical Res.*, 84(4), 1809–1826.
Shore protection manual. (1984). Coastal Engineering Research Center, U.S. Army Corps of Engineers, Vicksburg, Miss.
Tsai, C. H., Iacobellis, S., and Lick, W. (1987). "Flocculation of fine grain sediments due to uniform shear stress." *J. Great Lakes Res.*, 13(2), 135–146.
Vanoni, V. (1975). Sedimentation engineering. ASCE, New York, N.Y.
Water inventory of the Portage River and Sandusky River basins and adjacent Lake Erie tributary regions. (1966). Water Division, Ohio Department of Natural Resources, Fountain Square, Columbus, Ohio.
Ziegler, C. K., and Lick, W. (1988). "The transport of fine-grained sediments in shallow waters." *Environ. Geology Water Sci.*, 11(1), 123–132.

APPENDIX II. NOTATION

The following symbols are used in this paper:

A = area;
C_c = Chezy coefficient;
C_i = size class concentration;
E = erodability coefficient;
f = friction factor;
g = gravitational acceleration;
H = $\eta + h$;
h = water depth from still water level;
K_{si} = empirical coefficient dependent upon sediment type;
K_x = dispersion coefficient in x-direction;
K_y = dispersion coefficient in y-direction;
M_{di} = deposited sediment mass [(14)];
M_{ei} = eroded sediment mass [(13)];
mass_d = total mass deposited;
P_i = probability of particles remaining deposited [(9)];
S_{di} = deposition sink term [(7)];
S_{ei} = entrainment source term [(5) or (6)];
T_n = thickness increase from deposition [(15)];
T_s = significant wave period;
t_d = deposition integration time;
U = depth averaged velocity in x-direction;
V = depth averaged velocity in y-direction;
$\bar{V}$ = depth averaged velocity vector;
V_{si} = settling velocity [(8)];
α_i = coefficient of erodability;
Δt = time interval;
ε_{0i} = coefficient of erodability;
ρ_b = sediment bulk density;
ρ_s = particle density;
ρ_w = density of water;
τ_{cei} = critical erosion shear;
$\bar{\tau}_b$ = bed shear due to currents and waves [(10)];
$\bar{\tau}_c$ = bed shear stress due to currents [(11)];
τ_{cdi} = critical deposition shear stress; and
$\bar{\tau}_w$ = bed shear stress due to waves [(12)].

Subscript

i = class size of sediment particles; and
n = sediment layer in bed model.